

Flow-History-Dependent Behavior in Entangled Polymer Melt Flow with Multiscale Simulation

Takahiro MURASHIMA^{1,2} and Takashi TANIGUCHI^{1,2}

¹*Department of Chemical Engineering, Kyoto University, Katsura Campus, Nishikyo-ku, Kyoto 615-8510, Japan*

²*Core Research for Evolutional Science and Technology, JST, Kawaguchi, Saitama 332-0012, Japan*

E-mail: murasima@cheme.kyoto-u.ac.jp

(Received October 3, 2011)

Polymer melts represent the flow-history-dependent behavior. To clearly show this behavior, we have investigated flow behavior of an entangled polymer melt around two cylinders placed in tandem along the flow direction in a two dimensional periodic system. In this system, the polymer states around a cylinder in downstream side are different from the ones around another cylinder in upstream side because the former ones have a memory of a strain experienced when passing around the cylinder in upstream side but the latter ones do not have the memory. Therefore, the shear stress distributions around two cylinders are found to be different from each other. Moreover, we have found that the averaged flow velocity decreases accordingly with increasing the distance between two cylinders while the applied external force is constant. While this behavior is consistent with that of the Newtonian fluid, the flow-history-dependent behavior enhances the reduction of the flow resistance.

KEYWORDS: multiscale simulation, fluid particle simulation, coarse-grained simulation, memory effect

1. Introduction

Predicting flow of entangled polymer melts is difficult because the microscopic states of polymers depend on the flow history, namely the history of the experienced strain during the flow. Moreover, the quite large number of the degrees of freedom in the entangled polymer melt makes it difficult to build the constitutive equation that describes the relation among the stress tensor and the strain (or strain-rate) tensor in the entangled polymer melt. To overcome the difficulty existing in the flow prediction of entangled polymer melts, we have developed a new multiscale simulation [1] composed of the macroscopic fluid particle simulation [2, 3] and the microscopic entangled polymer dynamics simulation [4–8]. Using the fluid particle simulation where each fluid particle has a polymer simulator that describes the polymer states in the fluid particle itself, we can accurately consider the flow history of the fluid particle and the polymers in the fluid particle. The entangled polymer dynamics simulations [4–8] are based on reptation theory [9–11] where the dynamics of a polymer chain is constrained in a tube created by the surrounding polymers because of excluded volume effect and entanglements between polymers. Because each polymer chain in the entangled polymer dynamics simulation is described with the number of hypothetical entanglement points Z and the tube segments $r_j^s (j = 1, \dots, Z)$ connecting the entanglement points on the chain, we can decrease considerably large amount of the degrees of freedom into a manageable number of the degrees of freedom. The multi-scale simulation enables us to simulate the polymer melt flow with remaining the detailed information on the entangled states of polymers.

In Ref. [1], we have considered a flow around a cylindrical obstacle using the new method and found that the polymer states are different between the upstream region and the downstream region because of the flow-history-dependent behavior of the entangled polymer melt. In that work, we

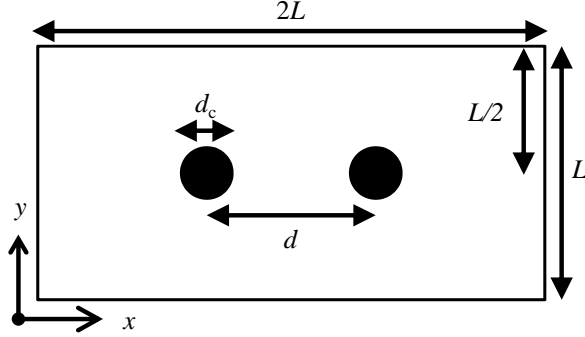


Fig. 1. Schematics of the system. Two infinitely long cylinders are placed in a rectangular system with an area $L \times 2L$. The length $L = 30a_0$ and the diameter $d_c = 6a_0$ of both cylinders are fixed where a_0 is the unit length of the macroscopic fluid simulation. The distance d between two cylinders is a constant parameter. The x -axis is chosen to be parallel to the flow direction and the y -axis is vertical to the x axis. Because of the translational symmetry towards the z -direction perpendicular to the x and y axes, we can focus on the two dimensional flow at the macroscopic level. When $d = L$, this system corresponds to the one considered in Ref. [1].

considered the case that there is only one cylinder in the system. If there are two cylinders in the system as shown in Fig. 1, the flow history in the upstream region will affect the polymer states in the downstream region. Moreover, we expect that the distance d between two cylinders can affect the flow behavior of entangled polymer melt. Because the cylinders are placed in tandem along the flow direction, the effect of the memory of the flow history can depend on the distance d between the cylinders. The purpose of the present paper is to clearly show the flow-history-dependent behavior of entangled polymer melt and to investigate the effect of the memory of the flow history using the new multiscale simulation [1].

2. Multiscale Simulation

In the multiscale simulation employed here, the polymer melt is described with an amount of fluid particles. The position \mathbf{r}_i and the velocity \mathbf{v}_i of the i -th fluid particle are updated according to the following equations:

$$\frac{d\mathbf{r}_i}{dt} = \mathbf{v}_i, \quad (1)$$

$$\rho_i \frac{d\mathbf{v}_i}{dt} = -\nabla p_i + \nabla \cdot \boldsymbol{\sigma}_i + \mathbf{f}, \quad (2)$$

where \mathbf{f} is an external body force with $\mathbf{f} = (f_x, 0)$. These equations are integrated with the velocity-Verlet algorithm. The spatial derivative of a field variable ∇f is calculated with the modified smoothed particle hydrodynamics (MSPH) algorithm [2, 3]. The density ρ_i at i -th fluid particle is calculated with the usual smoothed particle hydrodynamics (SPH) [12] technique: $\rho_i = \sum_{j \in \Omega_i} m_0 W(|\mathbf{r}_i - \mathbf{r}_j|, h)$ where $W(r, h)$ is a Gaussian function with a cutoff length $2h$ [2]. The pressure p_i is a function of ρ_i . The stress tensor $\boldsymbol{\sigma}_i$ depends on the microscopic states of polymers simulated with the polymer dynamics simulation. Using the dual-slip-link model (DSLML) [5, 6] as the microscopic simulation in the multiscale simulation, we can obtain the polymeric stress $\boldsymbol{\sigma}^p$ coming from the entangled polymer states. DSLML can describe the polymer dynamics larger than the tube diameter b . To include the faster dynamics than the tube dynamics (or the dynamics less than the tube diameter), we supply the dissipative stress $\boldsymbol{\sigma}^d$ to the stress tensor $\boldsymbol{\sigma}$. Because the relaxation time of such faster dynamics is negligibly small compared to the tube dynamics, we can regard the dissipative stress $\boldsymbol{\sigma}^d$ as a

Newtonian stress tensor with a constant viscosity η^d . Then, the stress tensor σ_i is assumed to be the sum of σ^p and σ^d :

$$\sigma_i = \sigma_i^p + \sigma_i^d. \quad (3)$$

The polymeric stress σ_i^p is obtained from DSLM as follows:

$$\sigma_i^p = \sigma_0 \left\langle \sum_{j=1}^Z \frac{\mathbf{r}_j^t \mathbf{r}_j^t}{|\mathbf{r}_j^t| b} \right\rangle_i, \quad (4)$$

where Z is the number of entanglements in a polymer chain, \mathbf{r}_j^t is the j -th tube segment vector on the chain, and $\sigma_0 \equiv (\eta^p/\eta^{p0})\sigma_e$ is the stress coefficient that transforms the stress unit σ_e in the microscopic simulation to that in the macroscopic simulation through the ratio η^p/η^{p0} . The bracket $\langle \cdots \rangle_i$ means the average over the polymer chains in the i -th fluid particle. The dissipative stress σ^d is assumed to be proportional to the deformation rate tensor \mathbf{D} as follows:

$$\sigma_i^d = \eta^d \mathbf{D}_i, \quad (5)$$

where η^d is the dissipative viscosity and $\mathbf{D}_i \equiv \nabla \mathbf{v}_i + (\nabla \mathbf{v}_i)^T$.

The macroscopic fluid particle simulation and the microscopic polymer dynamics simulation communicate with each other through the following procedure:

- (1) $\kappa_i \equiv (\nabla \mathbf{v}_i)$ is calculated in the fluid particle simulator using MSPH algorithm.
- (2) κ_i is transferred to the polymer simulator.
- (3) The polymer states, namely $\{Z\}$ and $\{\mathbf{r}_j^t\}$, subjected to κ_i are updated for Δt in the polymer simulator.
- (4) σ_i^p is calculated using Eq. 4
- (5) σ_i^p is transferred to the fluid particle simulator.

The process (3) is composed of several steps, shortly explained as follows (for more information, see Ref. [6]):

- (3.1) Subjected to κ_i , the tube segments $\{\mathbf{r}_j^t\}$ are affinely deformed.
- (3.2) The updated chain length $l = \sum_{j=1}^Z |\mathbf{r}_j^t| + s_1 + s_2$ is relaxed only for a time interval Δt where s_1 and s_2 are the lengths of end-segments of the polymer chain out of the tube; The relaxation dynamics is composed of the reptation motion and the chain retraction where the equilibrium length of the polymer chains, $l_{eq} \equiv \langle Z \rangle_{eq} b$, is assumed.
- (3.3) The number of entanglement Z is renewed depending on the length of s_i ($i = 1, 2$). When s_i is larger than b , a new tube segment with a length b is created at the end of the chain in s_i side, and b is subtracted from s_i . At the same time, a new entanglement point is created in the other polymer chain randomly selected. This new entanglement point and the new end of the polymer tube are coupled with each other, which mimics the entanglement between the polymer chains. When s_i is less than 0, the entanglement at the end of the polymer tube is erased and the entangled pair is also erased, which mimics the disentanglement process (constraint release).

The procedure from (1) to (5) is the most time-consuming part in the multiscale simulation due to the excessively large number of degrees of freedom coming from the large number of fluid particles each having the large number of internal degrees of freedom. However, because the procedure from (1) to (5) is independent of the other fluid particles, parallel computing drastically improves the time-efficiency of the multiscale simulation.

Table I. Fixed parameters in this article (cf., Ref. [1]).

t_0	1.0	Unit time in the macroscopic simulation
a_0	1.0	Unit length in the macroscopic simulation
m_0	1.0	Unit mass in the macroscopic simulation
t_e	(= t_0) 1.0	Unit time in the microscopic simulation
a_e	(= $b \ll a_0$) 1.0	Unit length in the microscopic simulation (Tube diameter)
σ_e	1.0	Unit stress in the microscopic simulation
Δt	$1.0 \times 10^{-2} t_0$	Time-integral step
$\langle Z \rangle_{\text{eq}}$	7.0	Average number of entanglements in equilibrium
$\eta^{\text{p}0}$	$17.5 \sigma_e t_e$	Zero-shear viscosity of entangled polymer melt when $\langle Z \rangle_{\text{eq}} = 7$ [1]
τ_d	$200 t_e$	Disentanglement time (Reptation time) when $\langle Z \rangle_{\text{eq}} = 7$ [1]
η_0	(= $\eta^{\text{p}} + \eta^{\text{d}}$) $1.0 m_0 / (a_0 t_0)$	Total zero-shear viscosity of the macroscopic flow
η^{p} / η_0	0.9	Viscosity ratio of polymeric viscosity
η^{d} / η_0	0.1	Viscosity ratio of dissipative viscosity
f_x	$5.0 \times 10^{-4} m_0 / (a_0^2 t_0^2)$	External body force
L	$30 a_0$	System length
d_c	$6.0 a_0$	Diameter of the cylinders
N_f	1,784	Total number of fluid particles
N_p	1,000	Number of polymer chains in a fluid particle
N_c	24	Number of fluid particles that represent the perimeter of a cylinder

The cylinder is represented with the N_c fluid particles evenly placed on the perimeter. These fluid particles fixed on the space also have their own polymer simulator that guarantees the non-slip boundary condition assumed on the interface between the polymer melt and the wall [13].

The parameters used in the present work are summarized in Table I. Using these parameters, we have found that the Reynolds number $\text{Re} = \rho U d_c / \eta_0$ is about 0.3 and the Deborah number $\text{De} = U \tau_d / d_c$ is about 1.8 where U is the average flow velocity in the system and is set to $0.055 a_0 / t_0$ when $d = 30 a_0$ (cf., Ref. [1]).

3. Results and Discussions

Now we investigate entangled polymer melt flows in the system shown in Fig. 1 using the multiscale simulation. At first, we focus on two different cases (a) and (b) where the distances between two cylinders are (a) $d = 10 a_0$ and (b) $d = 20 a_0$ (cf., Ref [1] when $d = 30 a_0$). As is the case in Ref. [1], we focus on the magnitudes of the velocity field $|\mathbf{v}|$, the shear deformation rate field $|D_{xy}|$, and the shear stress field normalized by the total zero-shear viscosity $|\sigma_{xy}| / \eta_0$. The fluid particle data are transformed into the data on the square lattice mesh using the linear interpolation method. Then, to decrease the noise of the data, we take an average of the obtained data over the time interval from $2,000 t_0$ to $3,000 t_0$ in the steady state, because the macroscopic states of flow have reached steady states before $1,000 t_0$ in this system.

The spatial distributions of these data are shown in Fig. 2. Comparing these two cases, as we expected, the flow-history-dependent behavior is clearly appeared in the shear stress distribution in (a) where the magnitude of the shear stress field around the cylinder in the upstream side is clearly different from that around the other cylinder in the downstream side, while it is difficult to observe such a behavior in (b). Moreover, focusing on the velocity fields in (a) and (b), the average flow velocity U in (a) seems to be higher than that in (b) because the high velocity region in (a) is broader than that in (b).

To clarify the relationship between U and d , we plot the average flow velocity U against the distance d in Fig. 3 (a). For the comparison, the open circles represent the results in the Newtonian

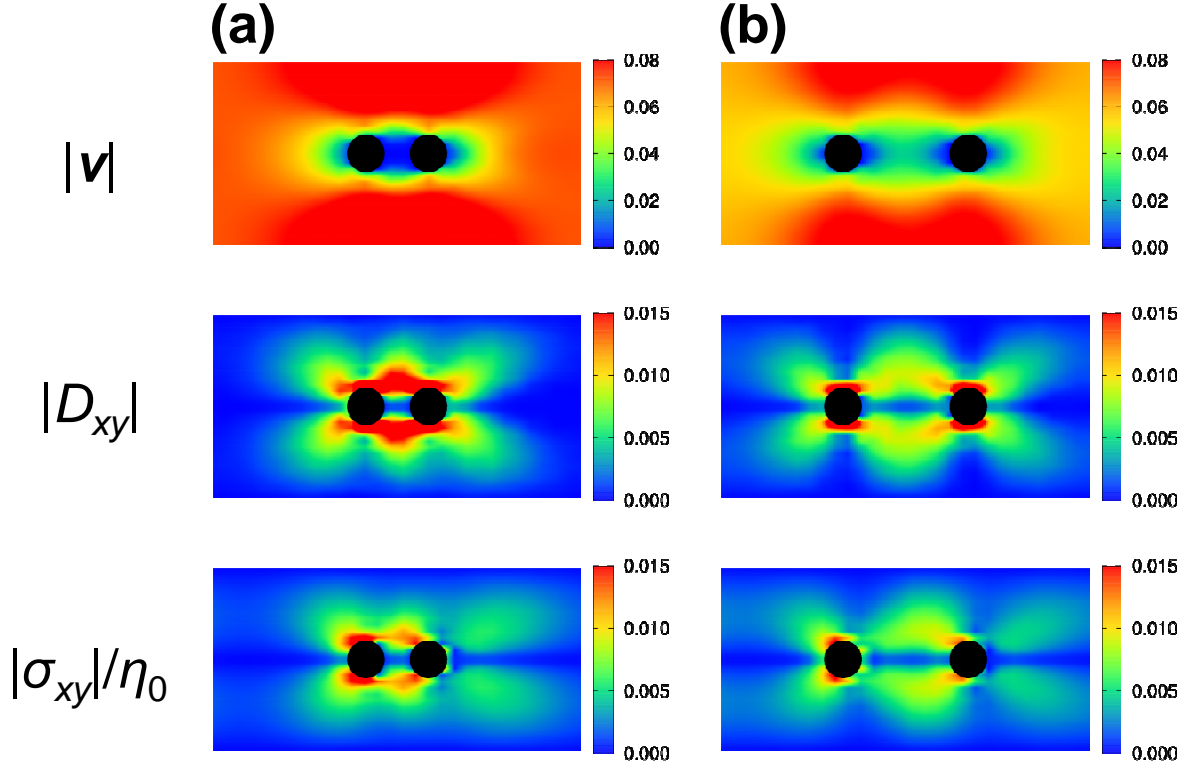


Fig. 2. Flow behaviors in cases of the distances (a) $d = 10a$ and (b) $d = 20a$ between two cylinders. The magnitudes of the velocity \mathbf{v} , the shear deformation rate D_{xy} and the shear stress normalized by the total zero-shear viscosity σ_{xy}/η_0 are shown here.

fluid ($\eta^d = \eta_0$ and $\eta^p = 0$). As shown in Fig. 3, the average flow velocity U decreases with increasing the distance d when $d < 30a_0$. Because of the periodicity of the system, the figure shows a symmetry on the line $d = 30a_0$, namely the configuration of the cylinders with the distance d for $d > 30a_0$ corresponds to that for $|d - 30a_0|$. Normalizing U and d as $U' = (U(d) - U(30a_0))/U(30a_0)$ and $d' = |d - 30a_0|/30a_0$, U' shows a monotonic increasing behavior with d' as shown in Fig. (b). The solid line and the dashed line in Fig. (b) are fitting lines obtained using the nonlinear least squares fitting. The shapes of these fitting curves are $U'(d') = c_P d'^{\alpha_P}$ where $c_P = 1.411 \pm 0.016$ and $\alpha_P = 2.979 \pm 0.035$ for the polymer melt flow and $U'(d') = c_N d'^{\alpha_N}$ where $c_N = 0.857 \pm 0.014$ and $\alpha_N = 2.969 \pm 0.051$ for the Newtonian flow. Comparing these results, the normalized flow velocity U' of the polymer melt is clearly enhanced with increasing d' , and the powers of the fitting functions for the polymer and Newtonian flows, however, are found to have almost the same value; $c_P > c_N$ and $\alpha_P \approx \alpha_N \approx 3$. Namely, the flow-history-dependent behavior enhances the average flow velocity (or decreases the viscosity) but does not affect the exponent of the power law function in this flow system.

4. Summary

We have investigated entangled polymer melt flow around two cylinders in tandem in a two dimensional rectangular system, using the new multiscale simulation [1] that is composed of the macroscopic fluid particle simulation and the microscopic entangled polymer dynamics simulation. In the system, the polymer melt has represented the flow-history-dependent behavior in the shear stress distribution. We have found that the flow-history-dependent behavior causes the orientation of

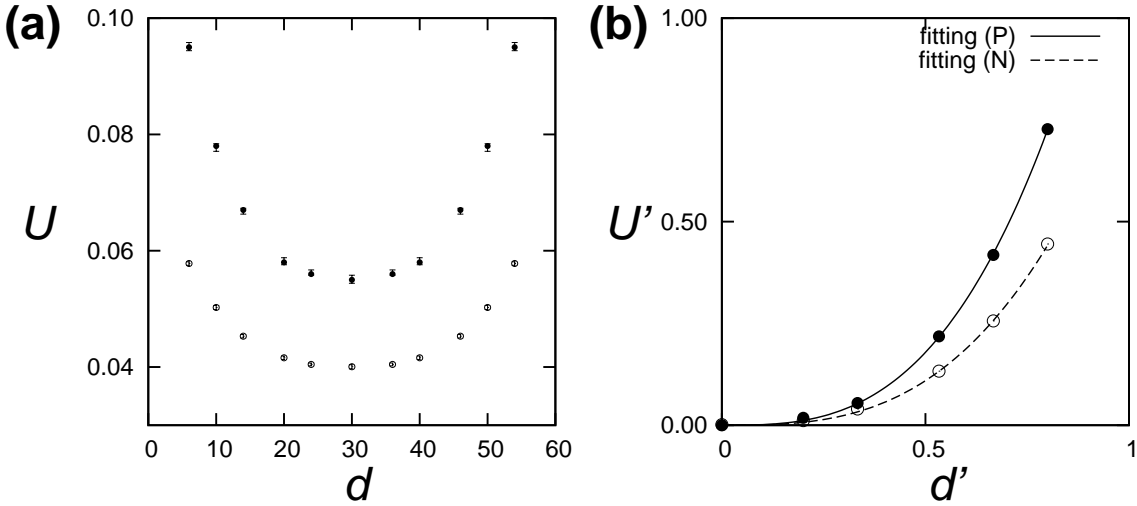


Fig. 3. The averaged flow velocity U and the distance d between two cylinders. The filled circles in the graph represent the polymer melt flow. For the comparison, the Newtonian flow results ($\eta^d = \eta_0, \eta^p = 0$) are also shown in the graph using open circles. When d is less than $30a$, the averaged flow velocity U decreases with increasing the distance d . Because of the periodicity of the system, this graph shows a symmetry on $d = 30a_0$, namely $U(d)$ for $d > 30a_0$ corresponds to $U(60a_0 - d)$. Normalizing U and d as $U' = (U(d) - U(30a_0)) / U(30a_0)$ and $d' = |d - 30a_0| / 30a_0$, the normalized velocity U' is found to be proportional to d'^3 both in the polymer melt flow and the Newtonian flow.

polymer chains, and then reduces the flow resistance. However, the flow history does not affect the exponent of the power law function obtained fitting the average flow velocity against the distance between cylinders.

References

- [1] T. Murashima and T. Taniguchi, *Europhys. Lett.*, **96** (2011) 18002.
- [2] G. M. Zhang and R. C. Batra, *Comput. Mech.*, **34** (2004) 137.
- [3] M. B. Liu, W. P. Xie, and G. R. Liu, *Appl. Math. Model.*, **29** (2005) 1252.
- [4] Y. Masubuchi, J. Takimoto, K. Koyama, G. Ianniruberto, G. Marrucci and F. Greco, *J. Chem. Phys.*, **115** (2001) 4387.
- [5] S. Shanbhag, R. G. Larson, J. Takimoto and M. Doi, *Phys. Rev. Lett.*, **87** (2001) 195502.
- [6] M. Doi and J. Takimoto, *Phil. Trans. R. Soc. Lond. A*, **361** (2003) 641.
- [7] A. E. Likhtman, *Macromol.*, **38** (2005) 6128.
- [8] T. Uneyama, *Nihon Reoroji Gakkaishi (J. Soc. Rheol. Japan)*, **39** (2011) 135.
- [9] S. F. Edwards, *Proc. Phys. Soc.*, **92** (1967) 9.
- [10] P. G. de Gennes, *J. Chem. Phys.*, **55**(1971) 572.
- [11] M. Doi and S. F. Edwards, *The theory of polymer dynamics*, Oxford University Press, (1986).
- [12] J. J. Monaghan, *Rep. Prog. Phys.*, **68** (2005) 1703.
- [13] So far, only non-slip boundary condition between the polymer melt and the wall is manageable in the present multiscale simulation. Substituting the bulk polymer simulator in the fluid particles fixed on the space to a simulator accounting for an interfacial dynamics among the polymer melt and the wall, we will be able to discuss the slip flow in the multiscale simulation. However, the slip behavior is observed in the very high Weissenberg number flow where $Wi \gg 1.0$, which far exceeds the flow ranges discussed in this work.